APPENDIX A

Sample synthesis and characterization

The tungstate phosphors $NaY(WO_4)_2$: x mol% Er^{3+} (x=0.5, 5) were synthesized via a high-temperature solid-state reaction method. The stoichiometric amounts (5g in total) of starting materials Na_2CO_3 (99.9%), Y_2O_3 (99.99%), Er_2O_3 (99.99%), and WO_3 (99.9%) were weight for preparing the target products. The above weight materials were mixed and grinded in an agate mortar for 30 min. The mixture was loaded into an alumina crucible and calcined at 1000 °C for 4h in an electric furnace.

In order to identify the phase purity and crystal structure of the obtained powder, the phase analysis of X-ray diffraction was detected via a Shimadzu XRD-600 (Japan), which equipped with a Cu-Ka1 radiation source (λ = 0.15406 nm). To confirm the fluorescence lifetimes of phosphor, the luminescence decay curve and near infrared emission spectra were measured under a xenon flash lamp excitation on Edingburgh FLS-1000 spectrometer (UK) and on Hitachi F-4600 (Japan). The diffuse reflection spectra were detected via a spectrophotometer Shimadzu UV-3600 (Japan), which equipped with an integrated sphere accessory Ante 206-23851-91 (China).

The XRD patterns of the final products are shown in Fig. A1 along with the diffraction pattern taken from the corresponding JCPDS card (NO. 48-0886). It can be found that the diffraction angle positions of the two samples are in accord with those of the JCPDS card, and no extra diffraction peaks are observed by comparing the diffraction patterns of studied samples with the standard pattern. These results obviously indicated that the target compounds $NaY(WO_4)_2$ were validated as pure phase, and the Er^{3+} doping did not vary the lattice of structure.

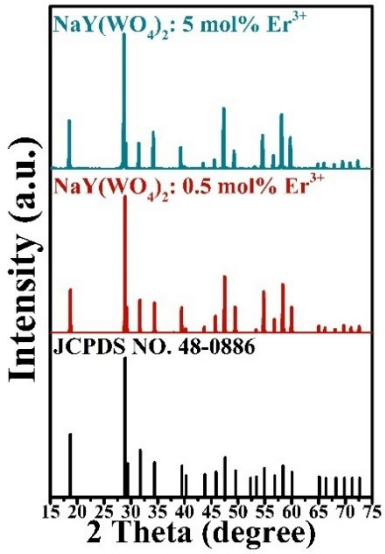

Fig. A1. XRD patterns of $NaY(WO_4)_2$: x mol% Er^{3+} (x=0.5, 5) and the standard pattern of corresponding JCPDS card (JCPDS NO. 48-0886)

The morphology and microstructure of the synthesized $NaY(WO_4)_2$: x mol% Er^{3+} (x=0.5, 5) phosphors were examined using scanning electron microscopy (SEM). The SEM images were obtained using a ZEISS GeminiSEM 300 (Germany) operating at an accelerating voltage of

3.00 kV and a working distance of 7.8 mm.

The SEM images reveal that the $NaY(WO_4)_2$: Er^{3+} phosphors exhibit irregular, polyhedral shapes with particle sizes varying widely. The majority of particles are estimated to range from approximately 2 μm to 20 μm in size, with some larger aggregates reaching beyond 20 μm. The particles possess relatively rough surfaces with noticeable microstructures and irregularities. This surface texture is likely a result of the high-temperature solid-state reaction process, which often leads to the formation of polycrystalline particles with varying degrees of surface roughness.

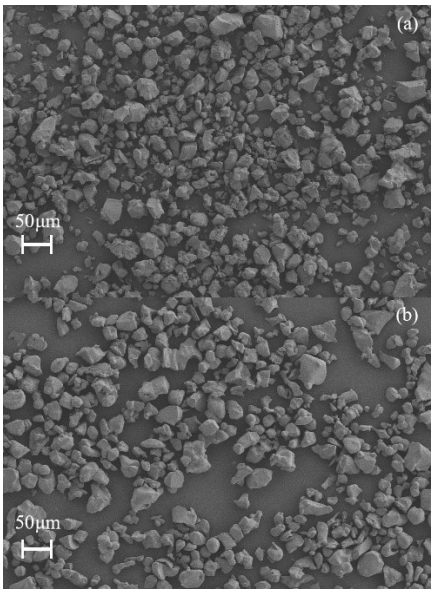

Fig. A2. SEM images of $NaY(WO_4)_2$: (a) 0.5 mol% and (b) 5 mol%Er^{3+} phosphors.

Subsequently, Fourier Transform Infrared (FTIR) spectroscopy was conducted to analyze the molecular vibrations and chemical bonds in the $NaY(WO_4)_2$: x mol% Er^{3+} (x=0.5, 5) samples. The FTIR spectra were recorded in the wavenumber range of 400 to 4000 cm^{-1}. The FTIR spectra, shown in Fig. A3, reveal significant absorption peaks at 925 cm^{-1}, 780 cm^{-1}, and 450 cm^{-1}. These peaks correspond to key vibrational modes[14-16]: The 925 cm^{-1} peak is likely associated with the W=O stretching vibration; The bands in the range of 400-800 cm-1 can be attributed to the W-O stretching and bending vibrations; These peaks are crucial indicators of the structural integrity of the WO_4 groups within the material. The high wavenumber region (1000-4000 cm^{-1}) exhibits a relatively stable transmittance, indicating that no significant molecular vibrations occur in this range. Despite the variation in Er^{3+} doping concentration, the positions of these peaks remain relatively consistent, indicating that the Er^{3+} ions have minimal impact on the local structural environment around the WO_4 groups. This observation aligns with the SEM analysis, where no notable changes in particle morphology were observed with varying Er^{3+} concentrations.

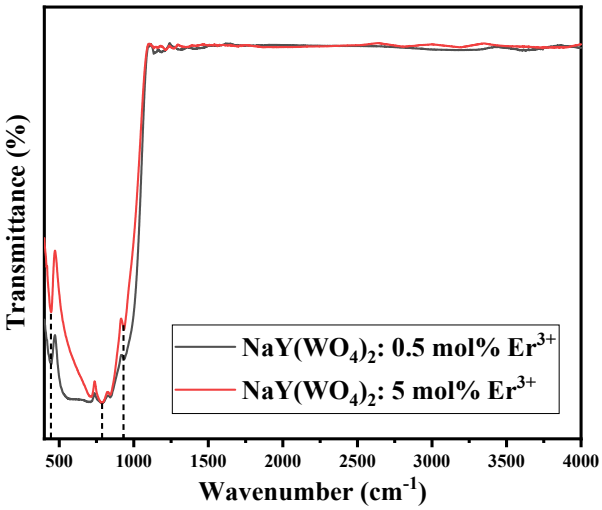

Fig. A3. FTIR spectra of $NaY(WO_4)_2$: x mol% Er^{3+} (x=0.5, 5).

APPENDIX B

Optical transition properties of Er^{3+} in $NaY(WO_4)_2$

In this section, in order to calculate the Judd-Ofelt parameters of Er^{3+} in $NaY(WO_4)_2$ and then to estimate the radiative transition rates, the refractive index of the host is required. In this work, the refractive index of $NaY(WO_4)_2$ will be confirmed from the dependence of refractive index on bandgap energy. Based on the Mott-Davis model, the relationship between the absorption coefficients $\alpha(hv)$ and the optical band gap energy E_{opt} can be expressed as [18],

$$\alpha(hv) = A(hv - E_{opt})^{1/2} \#(B1)$$

in which A is a constant which defines as the band tailing, and the meanings of the other symbols have already been given above. The $[\alpha(hv)]^2$- hv curve was plotted based on the absorption spectrum derived from the diffuse reflection spectrum and displayed in Fig.B1. The optical band gap energy can be confirmed by extending the linear absorption edge to the intersect with x-axis (viz $[\alpha(hv)]^2$=0). In Fig. B1, the red straight line stands for the extended line of the absorption edge, the dashed line represents the x-axis, and the optical band gap energy is the x coordinate value at the intersection point between two straight lines that equals 4.372 eV.

Subsequently, Moss, Dimitrov-Sakka, and Reddy models as expressed below were used to estimate the refractive index of $NaY(WO_4)_2$ [19-21].

$$n_{Moss} = \left(\frac{95}{E_{opt}}\right)^{0.25} \#(B2)$$

$$n_{D-S} = \left(6\sqrt{\frac{5}{E_{opt}}} - 2\right)^{0.5} \#(B3)$$

$$n_{Reddy} = \left(1 + \left(\frac{13.6}{E_{opt} + 3.4}\right)^2\right)^{0.5} \#(B4)$$

The values of n_{Moss}, n_{D-S} and n_{Reddy} derived from the optical band gap are 2.159, 2.102, and 2.015, respectively. The final used in the optical calculation value of the refractive index n was the average of three refractive indexes that equals 2.092.

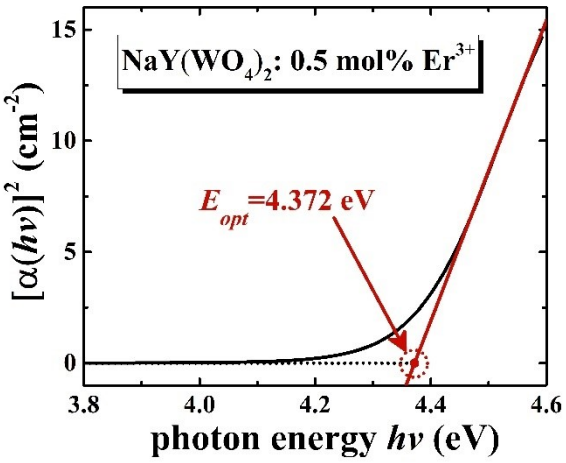

Fig. B1. $[\alpha(hv)]^2$- hv curve for $NaY(WO_4)_2$: 0.5 mol%Er^{3+}

In this work, the Judd-Ofelt parameters of Er^{3+} in $NaY(WO_4)_2$ compound will be calculated by a route that we proposed previously, and the optical transition rates will be estimated according to the Judd-Ofelt parameters in order to further confirm the cross sections. First, the diffuse reflection spectrum for the 5 mol% Er^{3+} doped $NaY(WO_4)_2$ sample was measured and is shown in Fig. B2 (a). Then, the relative absorption spectrum was calculated by the diffuse reflectance spectrum via the following Kubelka-Munk function and drawn in Fig. B2 (b)[22].

$$\alpha'(v) = C\frac{[1-R(v)]^2}{2R(v)} \#(B5)$$

where $\alpha'(v)$ stands for the relative absorbance at wavenumber v, $R(v)$ is the reflection ratio, and C is a constant independent from wavenumber. Besides, the relative experimental oscillator strength f_{exp}' and the theoretical electric dipole oscillator strength f_{th}^{ED} can be respectively calculated by the relative absorbance and the Judd-Ofelt theory via Eqs. B6 and B7 below.

$$f_{exp}' = \frac{mc^2}{\pi e^2}\int \alpha'(v)dv \#(B6)$$

$$f_{th}^{ED} = \frac{8\pi^2 mcv}{3h(2J+1)}\frac{(n^2+2)^2}{9n}\sum_{\lambda=2,4,6}\Omega_\lambda\left|\langle (S,L)J|U^\lambda|(S',L')J'\rangle\right|^2 \#(B7)$$

In the above equations, m represents the mass of single electron, c is the speed of light in vacuum, π stands for a circumference ratio, e is the charge of an electron, J is the angular moment quantum number of the initial state, Ω_λ(λ=2,4,6) are the Judd-Ofelt parameters and $\left|\langle (S,L)J|U^\lambda|(S',L')J'\rangle\right|$ is the reduced matrix element. For pure electric dipole transition, let the relative experimental and theoretical electric dipole oscillator strength in Eqs. (B6) and (B7) be equal. The observed transitions in Fig. B2 were used to establish a set of equations, and the solutions for the equations were found via a least square method, which is a set of nominal Judd-Ofelt parameters Ω'_λ(λ=2,4,6). It should be mentioned that the three transitions from the ground state $^4I_{15/2}$ to the excited states

$^4G_{9/2}$($^2K_{15/2}$, $^4G_{7/2}$) were not included in the Judd-Ofelt calculation since these transitions are weak, and could not be separated. The final obtained results of the relative experimental oscillator strengths f'_{exp}, the relative theoretical oscillator strengths f'^{ED}_{th}, and the absolute error δ_{rms} that estimated by equation below are displayed in Table B1.

$$\delta_{rms} = \left(\sum_{i}^{N} \frac{\left(f'_{expi} - f'^{ED}_{th\,i} \right)^2}{N-3} \right)^{1/2} \#(B8)$$

In above equation N is the transition number involved in this calculation, f'_{expi} and $f'^{ED}_{th\,i}$ stand for the relative experimental and theoretical oscillator strengths corresponding to i^{th} transition. According to Table B1, most of the oscillator strengths are bigger than the calculation error δ_{rms}, which imply that all the calculation procedures and results such as the relative Judd-Ofelt parameters Ω'_λ (λ=2,4,6) are reliable[23].

Table B1. Relative experimental and theoretical oscillator strengths and calculation error of Er^{3+} in $NaY(WO_4)_2$

Energy level	Experimental oscillator strengths	Theoretical oscillator strengths
	f'_{exp} (10^{-8})	f'^{ED}_{th} (10^{-8})
$^4I_{11/2}$	**31.488**	**38.496**
$^4I_{9/2}$	**25.272**	**39.696**
$^4F_{9/2}$	**194.844**	**189.924**
$^4S_{3/2}$	**21.36**	**12.648**
$^2H_{11/2}$	**1433.628**	**1412.292**
$^4F_{7/2}$	**115.488**	**99.504**
$^4F_{5/2}$, $^4F_{3/2}$	**21.96**	**23.964**
$^2H_{9/2}$	**29.592**	**28.272**
$^4G_{11/2}$	**2470.212**	**2488.116**
δ_{rms}	**12.44675**	

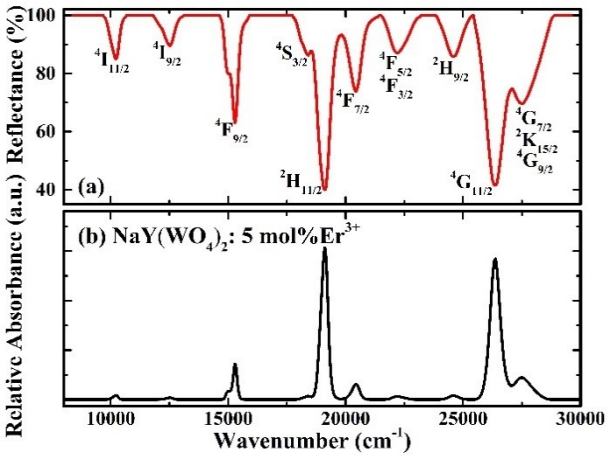

Fig. B2 Diffuse reflectance (a) and relative absorption (b) spectra for $NaY(WO_4)_2$: 5 mol% Er^{3+}

In order to determine the absolute values of Judd-Ofelt parameters, the radiative transition rate for a certain level of Er^{3+} needs to be confirmed. Therefore, the radiative transition of $^4I_{13/2} \rightarrow {}^4I_{15/2}$ of Er^{3+} was chosen to calibrate the relative values of Judd-Ofelt parameters. The relative electric dipole transition rate $A_{4_{I_{13/2}}}^{'ED}{}_{\rightarrow 4_{I_{15/2}}}$ can be calculated by the previously obtained relative Judd-Ofelt parameters via the following equation[24].

$$A_{4_{I_{13/2}}}^{'ED}{}_{\rightarrow 4_{I_{15/2}}} = \frac{64\pi^4 e^2 v^3 n\left(n^2+2\right)^2}{27h(2J+1)} \sum_{\lambda=2,4,6} \Omega_\lambda^{'} \left|\left\langle (S,L)J \middle| U^\lambda \middle| (S^{'},L^{'})J^{'} \right\rangle\right|^2 \#(B9)$$

Based on the selection rules for magnetic dipole transition $^4I_{13/2} \rightarrow {}^4I_{15/2}$, the magnetic dipole transition rate $A_{4_{I_{13/2}}}^{MD}{}_{\rightarrow 4_{I_{15/2}}}$ can be calculated from the function below[25].

$$A_{4_{I_{13/2}}}^{MD}{}_{\rightarrow 4_{I_{15/2}}} = \frac{16\pi^4 e^2 n^3}{3h(2J+1)m^2c^2} \left|\left\langle (S,L)J \middle| L+2S \middle| (S^{'},L^{'})J^{'} \right\rangle\right|^2 \#(B10)$$

In Eq. B10, $\left|\left\langle (S,L)J \middle| L+2S \middle| (S^{'},L^{'})J^{'} \right\rangle\right|^2$ represents the reduced matrix element for the magnetic dipole transition. Furthermore, the nonradiative transition rate and energy transfer rate starting from $^4I_{13/2}$ level are negligible at room temperature due to the low maximum phonon energy (about 900 cm^{-1}) and the very low doping concentration of Er^{3+} (0.5 mol%) [26]. Thus, the absolute total radiative transition rate $A_{4_{I_{13/2}}}^{RAD}$ of $^4I_{13/2}$ level is the sum of the absolute electric dipole and magnetic dipole transition rate and equals to the reciprocal of the fluorescence lifetime $\tau_{4_{I_{13/2}}}$, thus it can be concluded

$$\frac{1}{\tau_{4_{I_{13/2}}}} = A_{4_{I_{13/2}}}^{RAD} = A_{4_{I_{13/2}}}^{ED}{}_{\rightarrow 4_{I_{15/2}}} + A_{4_{I_{13/2}}}^{MD}{}_{\rightarrow 4_{I_{15/2}}} \#(B11)$$

The fluorescence decay at 1539 nm was measured for $NaY(WO_4)_2$: 0.5 mol% Er^{3+} and is shown in Fig. B3 (black dots). The fluorescence decay can be approximated by a straight line in a logarithmic

coordinates system which implies that the energy transfer could be indeed excluded in the total radiative transition of $^4I_{13/2}$ level. The fluorescence lifetime was obtained by single-exponential fitting to be 3.79 ms. From Eq. B9, the relative electric dipole transition rate $A_{^4I_{13/2}\overset{'ED}{\rightarrow}{}^4I_{15/2}}$ have already obtained via the relative Judd-Ofelt parameters and was linearly related to the Judd-Ofelt parameters. Finally, the absolute Judd-Ofelt parameters Ω_λ can be calculated from Eq. B12 by the ratio of the relative and absolute electric dipole transition rates as follows.

$$\Omega_\lambda = \frac{A_{^4I_{13/2}\overset{ED}{\rightarrow}{}^4I_{15/2}}}{A'_{^4I_{13/2}\overset{ED}{\rightarrow}{}^4I_{15/2}}}\Omega'_\lambda \#(B12)$$

The absolute Judd-Ofelt parameters Ω_2, Ω_4 and Ω_6 are derived to be 12.04, 2.65 and 0.41 in 10^{-20}cm^2, respectively. **The Judd-Ofelt parameters for Er^{3+} in $NaY(WO_4)_2$ obtained via above-presented procedure are listed in Table B2, and meanwhile the Judd-Ofelt parameters of Er^{3+} in the same and other molybdates reported in literatures were also listed for comparison purpose. Based on the data presented in Table B2, it is evident that the Judd-Ofelt parameters obtained for Er^{3+} in NaY(WO4)2 are in close agreement with those reported for similar materials in the literature. This further validates the accuracy of the method employed in this study.**

Table B2. Comparison of the Judd-Ofelt parameters of Er^{3+}

	Status	Ω_2	Ω_4	Ω_6	Ref.
		(10^{-20}cm^2)			
$NaY(WO_4)_2$:Er	**Powder**	**12.04**	**2.65**	**0.41**	**This work**
$NaLa(WO_4)_2$: Er/Ce/Yb	***Single crystal***	***15.31***	***3.07***	***1.30***	***[27]***
$NaGd(WO_4)_2$: Er	***Powder***	***12.07***	***3.58***	***0.86***	***[28]***
$NaGd(WO_4)_2$: Er	***Single crystal***	***14.91***	***2.19***	***1.30***	***[29]***

Then the electric dipole and magnetic radiative transition rates for Er^{3+} in $NaY(WO_4)_2$ compound was calculated by the absolute Judd-Ofelt parameters via Eqs. B9 and B10. The fluorescence branching ratios $\beta_{J\rightarrow J'}$ and radiative transition lifetimes τ_J were also determined via the following equations and are listed in Table B3. The data obtained in section will be used for confirming the cross-sections.

$$\beta_{J\rightarrow J'} = \frac{A^{RAD}_{J\rightarrow J'}}{\sum_{J'} A^{RAD}_{J\rightarrow J'}} \#(B13)$$

$$\tau_J = \frac{1}{\sum_{J'} A^{RAD}_{J\rightarrow J'}} \#(B14)$$

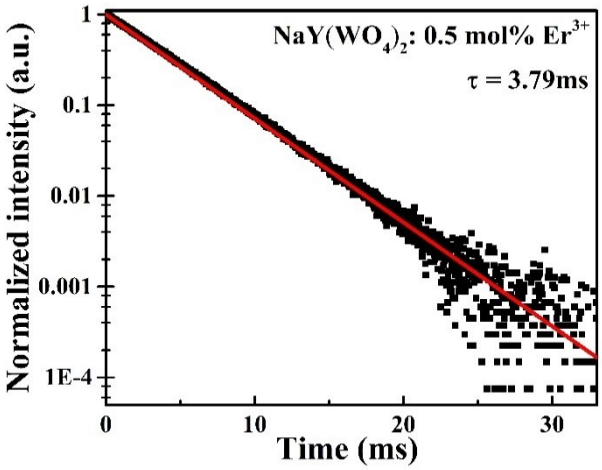

Fig. B3. Fluorescence lifetime of $^4I_{13/2}$ level in $NaY(WO_4)_2$: 0.5 mol% Er^{3+}.

Table B3. Oscillator strengths, radiative transition rates, branching ratios and radiative lifetimes of Er^{3+} in $NaY(MoO_4)_2$.

Initial level	Final level	Oscillator strengths		Radiative transition rates		Branching ratios	Radiative lifetimes
		f^{ED} (10^{-8})	f^{MD} (10^{-8})	A^{ED} (s^{-1})	A^{MD} (s^{-1})	β (%)	τ (μs)
$^2H_{11/2}$	$^4S_{3/2}$	1.52		0.12		0.00	25
	$^4F_{9/2}$	129.10		147.26		0.37	
	$^4I_{9/2}$	64.72		430.96		1.08	
	$^4I_{11/2}$	11.50		322.74		0.81	
	$^4I_{13/2}$	4.34		514.18		1.28	
	$^4I_{15/2}$	2467.90		38655.47		96.47	
$^4S_{3/2}$	$^4F_{9/2}$	0.03		0.47		0.03	673
	$^4I_{9/2}$	14.53		105.54		7.10	
	$^4I_{11/2}$	1.18		40.48		2.72	
	$^4I_{13/2}$	32.64		382.25		25.71	
	$^4I_{15/2}$	21.66		957.83		64.43	
$^4F_{9/2}$	$^4I_{9/2}$	11.63		21.69		0.49	226
	$^4I_{11/2}$	21.29		132.90		3.01	
	$^4I_{13/2}$	13.42		250.43		5.67	
	$^4I_{15/2}$	318.73		4010.12		90.83	
$^4I_{9/2}$	$^4I_{11/2}$	1.18	37.14	2.23	5.72	1.29	1623
	$^4I_{13/2}$	28.16		43.30		7.03	
	$^4I_{15/2}$	19.53		564.84		91.68	
$^4I_{11/2}$	$^4I_{13/2}$	39.93	63.69	33.19	23.51	15.98	2818
	$^4I_{15/2}$	14.42		298.15		84.02	
$^4I_{13/2}$	$^4I_{15/2}$	97.42	77.83	161.59	102.07	100.00	3793